Efficient hole transport material composite based on poly(3-hexylthiophene) and bamboo-structure carbon nanotubes for high performance perovskite solar cells

Molang Cai, Vincent Tiing Tiong, Tubuxin Hreid, John Bell, Hongxia Wang*

Corresponding author: hx.wang@qut.edu.au

Abstract : In this work, we have developed a new efficient hole transport material (HTM) composite based on poly(3-hexylthiophene) (P3HT) and bamboo-structure carbon nanotubes (BCN) for $CH_3NH_3PbI_3$ ($MAPbI_3$) based perovskite solar cells. Compared to pristine P3HT, it is found that the crystallinity of P3HT was significantly improved by addition of BCN, which led to over one order of magnitude higher conductivity for the composite containing 1-2wt% BCN in P3HT. In the meantime, the interfacial charge transfer between the $MAPbI_3$ light absorbing layer and the HTM composite layer based on the P3HT/BCNs was two-fold faster than pristine P3HT. More importantly, the HTM film with superior morphological structure consisting of closely compact large grains was achieved with the composite containing 1wt% BCNs in P3HT. The study by electrochemical impedance spectroscopy has confirmed that the electron recombination in the solar cells was reduced nearly ten-fold with the addition of 1wt% carbon nanotubes in the HTM composite. Owing to the superior HTM film morphology and the significantly reduced charge recombination, the energy conversion efficiency of the perovskite solar cells increased from 3.6% for pristine P3HT to 8.3% for P3HT/(1wt% BCNs) with a significantly enhanced open circuit voltage (V_{oc}) and fill factor (*FF*). The findings of this work are important for development of new HTM for high performance of perovskite solar cells.

Introduction

Solar cells based on organic-inorganic methylamonium lead halide perovskite compound ($CH_3NH_3PbX_3$, X= Cl, Br, I, $MAPbX_3$) have attracted significant attention because of their promise for cost-effective solar electricity compared to traditional crystalline silicon solar cells.[1-6] Generally speaking, a perovskite solar cell (PSC) consists of three main components with 1) a n-type semiconductor such as TiO_2 which serves as a scaffold for electron transport; 2) $MAPbX_3$ perovskite based light absorber material; and 3) a hole transport material (HTM) which is interfaced with the MAPbX3 material for charge separation and subsequent hole transport. The performance of a PSC depends on the light harvesting efficiency of the light absorber material, the charge separation efficiency at the interface of $MAPbX_3$/HTM and the charge transport efficiency in both HTM and $MAPbX_3$ layer. Until now, the majority study in the area of PSCs has been focus on the $MAPbX_3$ perovskite light absorber, attempting to understand its underlying properties and to improve its stability in PSC devices.[7-11]

Nevertheless a HTM with efficient hole transport mobility is equally critical for high performance PSCs. Actually the first $MAPbX_3$ (X= I, Br, Cl) based solar cells produced a power conversion efficiency (η) of only 3.8% as reported by Kojima *et al* in 2009.[12] The breakthrough was made by Lee *et al* by replacing the liquid electrolyte containing hole transport species with solid state HTM based on 2,2',7,7'-tetrakis(N,Ndi-p-ethoxyphenylamino)-9,9'-spirobifluorene (Spiro-OMeTAD), which boosted the efficiency to 10.9% in 2012.[1]

Besides Spiro-OMeTAD, other types of HTM have been investigated for PSCs. [13-15] Among them, conjugated conductive polymer based on poly(3-hexylthiophene) (P3HT) is another widely used HTM in PSCs because of its solubility in variable solvents, which enable deposition of P3HT film using cost-effective solution-processing technique such as spin coating for solar cell fabrication. However, the performance of pure P3HT based PSCs is generally low. The current best reported PSCs efficiency with P3HT and $MAPbI_3$ is 4.5%.[16] According to Bi *et al*, the rather flat molecular structure of P3HT can cause more serious charge recombination processes and thus was responsible for the lower efficiency in PSC compared to the well-known spiro-OMeTAD based device.[16] In addition, in comparison to traditional inorganic semiconductors, P3HT has lower hole mobility with conductivity normally of the order of 10^{-5} S/cm due to its poor crystalline nature.[17] The low charge carrier mobility is detrimental to solar cells because it can cause high series resistance and significant recombination between electrons and holes in solar cells, thus reducing the performance of device.

As a semi-crystalline material, the charge transport in P3HT is determined by the conductive domains which consist of ordered crystallites.[18] Several approaches have been developed to improve the crystallinity and thus the hole transport mobility of P3HT. These include post-thermal annealing treatment or using various solvent as well as using additives such as carbon-based materials to improve the local crystalline order of P3HT.[19] Geng *et al* have

reported that addition of single-wall carbon nanotubes (SWNTs) can improve the crystallinity of P3HT due to nanotube-induced π-π stacking interaction. Such interaction results in local molecular orientation of P3HT in a nanoscale dimension along the wall of carbon nanotubes, which is beneficial to crystallization of polymer from its solution as the solvent evaporates.[20] The interaction between P3HT and SWNTs may even change the optical band gap of P3HT besides contributing the carrier mobility.[21] Similar phenomenon of improved crystallinity and modification of the band gap of P3HT has also been reported with multiwall carbon nanotubes (MWNTs).[22] In addition, the theoretical study has also confirmed that P3HT could self-assemble around carbon nanotubes (CNTs) through its main chain, which would enhance the conjugation in the blend and maximize the interfaces between P3HT and MWNTs.[23]

Besides charge transport, charge transfer at the interface between $MAPbX_3$ and HTM is also critical for the performance of solar cells. For high energy conversion efficiency, the photo-generated electron-hole pair needs to be separated efficiently to avoid recombination. Hence, the surface properties of the HTM layer are very important for efficient interfacial charge transfer in the device. However, little research is available on this key process so far.

In this work, a series of hole transport materials based on a composite of P3HT and bamboo-structured carbon nanotubes (BCN) have been developed for PSCs. It is found that both the open circuit voltage (V_{oc}) and fill factor *(FF*) of the PSCs were significantly enhanced with the addition of BCNs in P3HT. The V_{oc} of the PSC with P3HT/(1 wt% BCN) HTM composite was enhanced by 250 mV compared to the device without BCNs. In the meantime, the *FF* of the device was increased from 0.35 for pure P3HT to 0.52 for P3HT/(1wt% BCN). As a consequence, the performance of the PSCs was improved from 3.6% for pure P3HT to 8.3% for P3HT/(1wt% BCN) composites. This remarkable performance improvement of the solar cell is attributed to the reduced electron recombination at the interface of $MAPbI_3$/HTM with the presence of BCN and the superior morphological structure with reduced grain boundaries for hole transport in the HTM layer.

Experimental

Synthesis of methylamonium iodide

Unless otherwise stated, all materials were purchased from Sigma Aldrich and used as received. Methylammonium iodide (CH_3NH_3I) was synthesized according to literature.[12] Briefly, Methylammonium iodide was formed through mixing methylamine (CH_3NH_2) solution (40 wt% in absolute ethanol) with hydroiodic acid (HI, 57 wt % in water) under nitrogen atmosphere at room temperature. The white methyl ammonium iodide (CH_3NH_3I) crystals were collected by evaporation of the solution by a rotary evaporator.

Deposition of TiO_2 film on FTO substrate

The perovskite solar cells were fabricated by the following procedure. First, laser-patterned, fluorine doped tin oxide (FTO)-coated glass substrates (TEC15, Pilkington) were cleaned under ultra-sonication in NaOH aqueous solution, deionized water, ethanol and acetone for 15 mins in sequence. The substrates were then annealed at 510℃ for 15 min to remove any residual organic material. A TiO_2 compact layer with thickness around 20-40 nm was then deposited on the substrates by aerosol spray pyrolysis at 500℃ using a precursor solution of titanium diisopropoxide bis(acetylacetonate) in isopropanol (0.2 M).[24] After cooling to room temperature, the substrates were further treated in 0.05 M aqueous solution of $TiCl_4$ for 30 min at 70℃, then rinsed with deionized water and dried at 500 ^oC for 20 min.[25] After this, a mesoporous TiO_2 film consisting of 20 nm particles was deposited by spin coating a TiO_2 colloid solution at 5000 r.p.m. for 30 s. The solution was made by diluting a commercial TiO_2 paste (Dyesol 18NRT) in ethanol with weight ratio of 2:7. The TiO_2 film with thickness around 550 nm was sintered at 510℃ for 15 min before cooling to room temperature naturally.

Fabrication of perovskite solar cells

Deposition of the TiO_2/$MAPbI_3$ film and TiO_2/$MAPbI_3$/HTM film were carried out in an argon-filled glovebox. $MAPbI_3$ film was deposited by spin-coating PbI_2 based N,N-dimethylformamide solution (concentration: 462 mg/ml) on the mesoporous TiO_2 film followed by drying at 70℃ for 30 min. After cooling to room temperature, the films were dipped in a solution of CH_3NH_3I in 2-propanol (10 mg/ml) for 20 s and then rinsed with 2-propanol and dried at 70℃ for 30 min.

The solution for the hole transport material (HTM) was composed of P3HT (10 mg/mL), 4-*tert*-butylpridine (TBP, 0.2 M) and bis(trifluoromethane) sulfonimide lithium salt (0.06 M) and different concentration of bamboo-structure carbon nanotubes (BCNs) (0 wt%, 0.5 wt%, 1 wt% and 2 wt%) in 1,2-dichlorobenzene solvent. The HTM solution

was spin-coated on the $CH_3NH_3PbI_3/TiO_2$ films and dried at 120 °C for 30 min. Finally, a layer of gold (80 nm) was thermally evaporated on top of the HTM layer to form the back contact of perovskite solar cells.

For clarity, in the following sections, the composite containing different content of BCN is named as P3HT/(*x* wt% BCN) where x= 0, 0.5, 1, 2. At least ten cells with each HTM composite were made to test the reproducibility of the result and to calculate the standard deviation of the average performance.

Characterization

The conductivity of P3HT/BCNs composite was determined by a Van der Pauw four point probe using computer controlled source meter (KeithLink LRS4-T, Taiwan) at room temperature. The HTM film for the measurement was prepared by spin-coating the corresponding P3HT/solution on a clean glass substrate followed by drying in a glove box. The thickness of the film was determined by SEM and a profilometer.

The micro-Raman spectrum of the material was measured by Renishaw Raman spectrometer with laser excitation wavelength of 530 nm at room temperature. The UV-visible spectrum of the material was recorded on a UV-Vis spectrometer (Cary 50). The photoluminescence (PL) measurement was conducted with a fluorescence spectrometer (FLS 920, Edinburgh Instruments Ltd) at room temperature. The PL emission spectrum of the film samples with comparable thickness was measured by exciting the samples with a light beam from a 450 W Xe lamp at 445 nm and nanosecond flash laser beam at 377 nm, respectively. Time-resolved PL decay was measured at the wavelength for peak emission (740 nm for perovskite) using a nanosecond flash laser beam at 377 nm. The surface and cross-section morphology of the P3HT/BCNs films was imaged using a field emission scanning electron microscope (FESEM, JEOL 7001F) at an acceleration voltage of 10.0 kV. The high resolution transmission electron microscope (HRTEM) measurement and selected area electron diffraction patterns of the HTM composite were performed with a JEOL 2010 transmission electron microscope with an accelerating voltage of 200 keV. The small angle X-ray diffraction (XRD) pattern of the material was recorded by X-ray diffract meter (Rigaku D max-2500, Japan) equipped with graphite monochromatized Cu K radiation (k=1.5418 Å). A scan rate of 8 ° min^{-1} in the 2θ range from 2 ° to 10 ° was used in the XRD measurement.

Electrochemical impedance spectroscopy (EIS) of the PSC was measured in the frequency range from 5 KHz to 1 Hz using an electrochemical workstation (VSP BioLogic Science Instruments) at a forward bias of -0.8V in dark. An AC voltage with perturbation amplitude of 10 mV was used in the EIS measurement. An equivalent circuit including a transmission line was used to fit the EIS results.[26]

The photocurrent density-voltage (*J-V*) characteristics of the solar cells was measured by recording the current as a function of applied voltage under the radiation of 100 mW/cm^2 (AM1.5) provided by a Xe lamp (150 W) based solar simulator (Newport). The cell was scanned from short circuit to open circuit. The illumination intensity of the solar simulator was calibrated with a monocrystalline reference silicon solar cell (Fraunhofer ISA). The active area of each cell was 0.09 cm^2.

Results and Discussion

Figure 1(a) shows the HR-TEM image of the carbon nanotubes. As can be seen, the nanotubes are very long with length up to several micrometres. The diameter of the tubes is around 10 nm and both end-opened and end-closed tubes are observed in the material. Many knots/joints can be seen clearly inside the tubes, making the nanotubes adopt a bamboo-like structure. The Raman spectrum of the nanotubes (Figure 1(b)) suggests that the bamboo-like carbon nanotubes (BCN) contains both single wall and multiwall nanotubes. The two main peaks at 1346 cm^{-1} and 1581 cm^{-1} in the Raman spectrum belong to the characteristic D and G vibration of carbon nanotubes respectively.[27] The D band is related with the defect induced disorder property of the carbon nanotubes while the G band originates from the splitting of E_{2g} in the graphite-like materials and is a characteristic mode of single wall carbon nanotubes.[28] The Raman peaks in the longer wavenumber are usually associated with the degree of crystallinity of the carbon nanotubes. It has been reported that single wall carbon nanotubes (SWNTs) behave differently than multiwall nanotubes (MWNTs) in contact with polymer such as P3HT. Generally speaking, SWNTs are more effective in enhancing the crystallization of the

polymer[29] whereas MWNTs have a greater effect on the conductivity of the polymer.[30,31] Hence, it is expected that the BCN here possess the merits of both SWNTs and MWNTs.

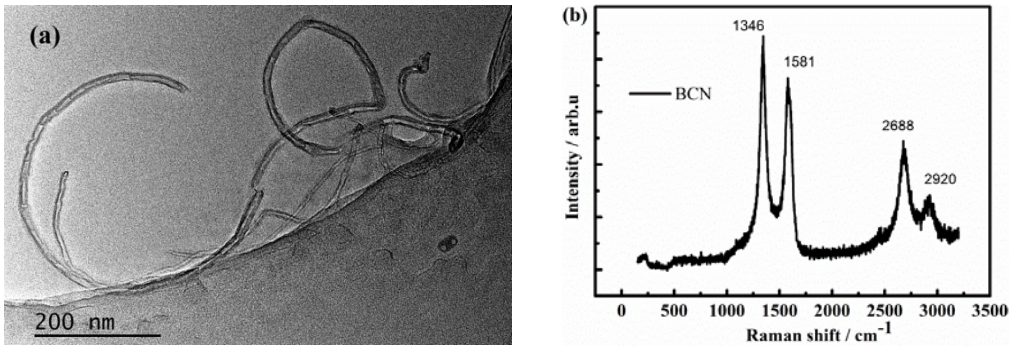

Figure 1. TEM image (a) and Raman spectrum (b) of bamboo-structure carbon nanotubes (BCN)

The HR-TEM image of the composite based on P3HT/(0.5wt% BCN) (Figure 2(b)) indicates that, compared to the pristine P3HT material which exists in the form of many needle-shape bundles (Figure 2(a)), the composite consists of a continuous network formed by the carbon nanotubes and P3HT. The surface of each carbon nanotube is fully covered with a layer of P3HT. This phenomenon is consistent with the previous reports by other researchers with P3HT/nanotube system. [22,27,32] Since some of the nanotubes are open-ended in our case, it is possible that the inside wall of the tubes could be covered by P3HT polymer as well. The thickness of the P3HT layer on the outer surface of BCN varies in the range of 2-10 nm. The networking structure of P3HT/carbon nanotubes has been reported to favour transfer of charge from P3HT to carbon nanotubes and subsequent transportation of charge along the nanotubes.[33] According to Geng *et al*,[20] the intimate contact between P3HT and carbon nanotubes induced by the π-π or CH_2-π interaction facilitates the crystallization of P3HT. This is also confirmed in our case. As shown in the selected area electron diffraction patterns (SAED) of P3HT (Figure 2(c)), a blurred diffraction ring with a *d* spacing = 0.12 nm is observed in the SAED pattern of pristine P3HT which is attributed to the (13, 0, 0) plane of P3HT crystals (JCPDS Card 48-2040). In contrast, the diffraction ring for the same lattice plane of P3HT is much stronger in the composite based on P3HT/(0.5wt% BCN) (Figure 2(d)), suggesting improved crystallinity of P3HT. In addition to the (13, 0, 0) lattice plane, the non-continuous bright dots observed in the SEAD pattern of the P3HT/(0.5wt% BCN) composite can be assigned to the (020) plane of P3HT. The bright dots strongly suggest the formation of single crystals of P3HT in the composite. Meanwhile, a diffraction ring corresponding to the (100) plane of the BCN is also detected by the SAED of the composite.

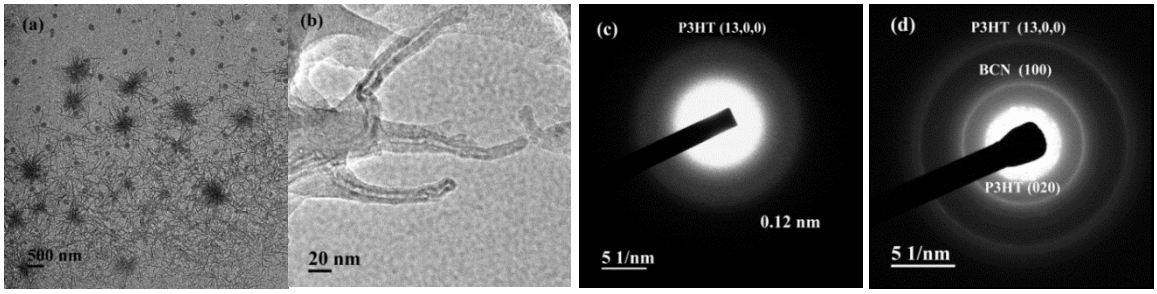

Figure 2. HRTEM pictures for (a) P3HT (b) P3HT/(0.5w% BCN) and corresponding selected area diffraction pattern (c) P3HT (d) P3HT/(0.5w% BCN).

The improved crystallinity of P3HT induced by different BCN content was further confirmed by XRD and UV-visible spectroscopy (Figure 3 (a, b)). As shown in Figure 3(a), the pristine P3HT shows a relatively weak and broad XRD peak at $2\theta = 5.32^{o}$ which is assigned to the diffraction of the crystallographic plane of (100) of P3HT crystals. After addition of 0.5 wt% BCN to P3HT, the XRD peak becomes sharper and stronger, suggesting the transformation of P3HT from semicrystalline to crystalline. However, further increase the content of the BCNs up to 2 wt% does not change the intensity of the XRD peak significantly. This suggests that 0.5 wt% BCN content is sufficient to induce the crystallization of P3HT.

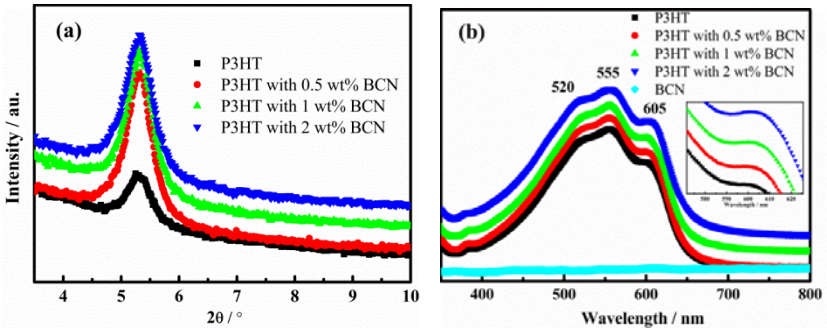

Figure 3. X-ray diffraction (XRD) patterns (a) and UV-visible absorption spectra (b) of P3HT/BCN composites containing different concentration of BCN.

The enhanced local crystalline order of P3HT is also reflected in the UV-visible absorption spectrum of the material as illustrated in Figure 3(b). The UV-visible light absorption of the BCN is also included in Figure 3(b) for comparison. Obviously, the BCN does not show observable light absorption in the spectrum range investigated. It is worth noting that all the UV-visible spectra of the HTM composites are normalized using the peak at 555 nm in order to see the evolution of other peaks clearly. Three peaks are observed in the UV-visible absorption spectrum. In particularly, the peak at 555 nm belongs to the vibronic absorption of extended conjugation lengths, resulting from the ordered packing of P3HT backbones which is normally observed in P3HT thin film.[34] The peak at 605 nm is the result of inter chain transition of P3HT and its intensity is correlated to the degree of local inter-chain order.[19] The higher is the crystalline order, the stronger is the intensity of this peak. As illustrated in inset of Figure 3(b), the peak intensity at 605 nm increases gradually with the increase of the content of BCN in the composite, suggesting the BCN addition improves the crystalline order of P3HT. This result is consistent with the results of XRD and SAED pattern of the materials. It is known that the high crystalline order benefits the charge transport in P3HT film which may reduce the series resistance of the film when used in PSCs.

To confirm this hypothesis, the charge transport properties of the P3HT/BCN composite films were investigated by measuring the conductivity of the film. As shown in Table 1, the conductivity of pristine P3HT based film is 1.56×10^{-4} S/cm, which is comparable to the literature value reported previously.[17] However, the conductivity is dramatically enhanced with the addition of BCN nanotubes. The addition of 0.5 wt% BCN in P3HT leads to nearly one order of magnitude enhancement of the conductivity. The conductivity is further increased to 8.65×10^{-3} S/cm with 1wt% BCN in the P3HT/BCN composite, a more than 50 times increase over pristine P3HT. Further increasing the BCN to 2wt% only increases the conductivity slightly. This result provides solid evidence that the charge transport in P3HT/BCN composite is improved compared to pristine P3HT. The lower series resistance of the HTM composite should have help improve the *FF* of corresponding PSC devices.

Table 1. Room temperature conductivity of P3HT/BCN composite with different content of BCN.

Films	σ(S/cm)
P3HT	1.56×10^{-4}
P3H/0.5wt% BCN	1.33×10^{-3}
P3HT/1wt% BCN	8.65×10^{-3}
P3HT/2wt% BCN	9.11×10^{-3}

Since a smooth, crystalline surface of HTM film is highly critical to establish a good interfacial contact with the adjacent $MAPbI_3$ perovskite layer in solar cells, thus the surface of the HTM film containing different content of BCN in P3HT was thoroughly examined (Figure 4). As shown in Figure 4(a), the surface of pristine P3HT based film is very rough and consists of grains with variable sizes. Many cracks appear in the film, indicating poor contact between the grains of P3HT. The small grains and cracks are very detrimental for the transport of charge carrier in the film. However, the surface of the HTM film is substantially improved by addition of BCN as indicated by the formation of grains which are connected with each other to form a smoother continuous film (Figure 4(b, c, d)). The new HTM film structure should favour charge transport because of reduced grain boundaries. The nanotubes which are integrated with the P3HT grains can also be seen clearly in the film surface. In particular, compared to all other films, the film based on the P3HT/(1wt% BCN) composite shows the best surface morphology with closely packed grains with least cracks. Beyond this value, further increase of the content of BCN to 2wt% leads to the increase of crack in the corresponding film again (Figure 4d). Hence, it is expected that, compared to other HTM materials investigated here, the film based on the P3HT/(1wt% BCN) composite should be most favourable for charge transport in the PSC device with reduced grain boundaries, and hence reducing electron recombination when used in PSCs devices.

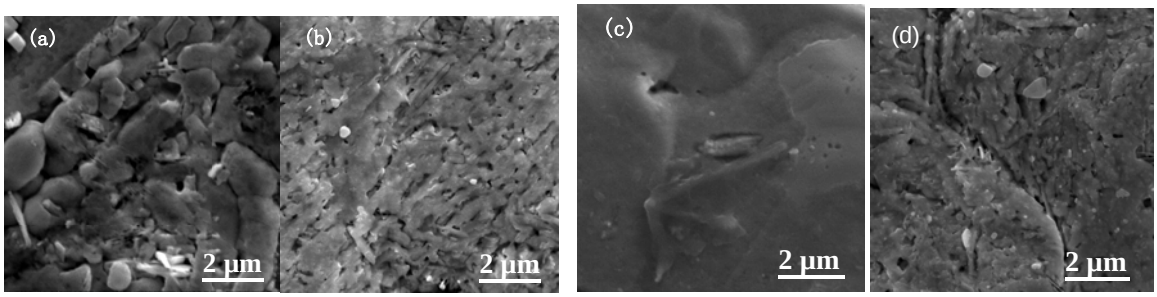

Figure 4. The SEM pictures of P3HT film containing different content of bamboo-structure carbon nanotubes (BCN): (a) no BCN (b) 0.5 w % BCN (c) 1 w % BCN (d) 2 w% BCN.

PSCs were then fabricated using the P3HT/BCN composites as HTM and their photovoltaic performance was evaluated. The cross-section image of one PSC device based on P3HT/(1wt% BCN) is illustrated in Figure 5 (a). A clear three layer structure consisting of TiO_2 coated perovskite light absorbing layer/HTM layer/Au electrical contact layer can be seen with the device. The thickness of the $MAPbI_3/TiO_2$ film and the HTM layer is around 550 nm and 220 nm respectively. It is noticed that around 150 nm of the HTM layer which penetrates into the $MAPbI_3/TiO_2$ mesoporous film to form an integrated structure for efficient interfacial charge transfer between the light absorbing material and the HTM can be clearly seen in the device.

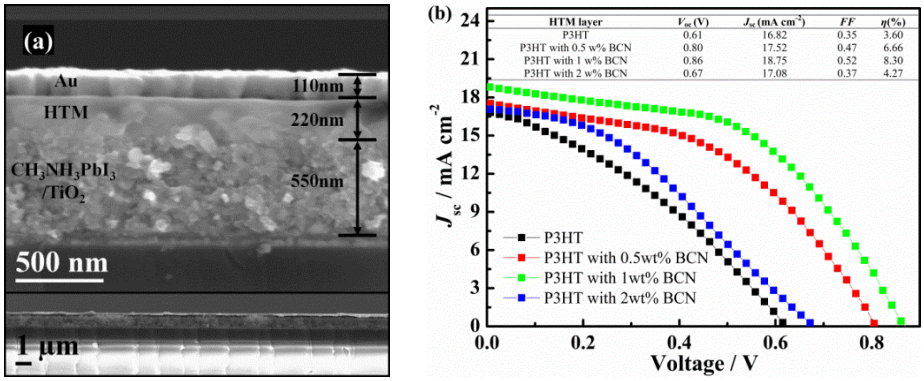

Figure 5. Cross-section image (a) and the *J-V* plots of the best performance (b) of perovskite solar cells containing different content of bamboo-structure carbon nanotubes (BCN) in P3HT.

Table 2. Photovoltaic parameters of perovskite solar cells with different content of BCN in P3HT*.

HTM layer	V_{oc} (V)	J_{sc} (mA cm^{-2})	*FF*	η (%)
P3HT	0.57±0.049	14.57±2.36	0.37±0.040	3.12±0.82
P3HT with 0.5 w% BCN	0.77±0.033	16.81±1.62	0.44±0.030	5.94±1.24
P3HT with 1 w% BCN	0.83±0.038	17.75±0.94	0.49±0.026	7.60±1.16
P3HT with 2 w% BCN	0.69±0.020	15.28±2.37	0.37±0.055	4.23±0.30

*The data shown are the average values obtained from 10 cells with standard deviation.

Figure 5(b) shows the photocurrent density (*J*) - photovoltage (*V*) curves and the corresponding characteristic performance parameters of the representative PSCs employing the prepared P3HT/ BCN composite with different content of BCN. An apparent striking feature in Figure 5(b) is that, compared to pristine P3HT based PSC device, the open circuit photovoltage (V_{oc}) of the P3HT/BCN composite based cells are significantly enhanced with the increase of BCN up to 1wt%. The V_{oc} of the cell increases from 0.61 V for P3HT to 0.86 V for P3HT/(1wt% BCN) composite. At the same time, there is a nearly 35% increase in the fill factor (*FF*) and 11% increase in J_{sc} of the P3HT/(1wt% BCN) composite compared to the device without BCN. As a consequence, the light to electricity conversion efficiency (η) of 8.3% is achieved with the PSC with P3HT/(1wt% BCN), which is over two fold higher than the performance of the pristine P3HT based solar cells (η = 3.6%). It should mention that at least ten cells for each type of HTM material containing different content of BCN in P3HT were made to test the reliability of the results. The average performance and the standard deviation of these cells are shown in Table 2. We are aware that a much higher energy conversion efficiency (9.3%) with P3HT based perovskite solar cells was reported by Giacomo *et al* using chloride doped perovskite compound ($MAPbCl_xI_{3-x}$). [35] For PSCs using MAPbI3 as light absorber and P3HT as HTM, the best efficiency that has been reported so far is 4.5%.[16] Thus, our base efficiency for P3HT (3.6%) is very reasonable. The much higher efficiency that was achieved in this work using P3HT/(1wt% BCN) composite has set a new milestone for this type of perovskite solar cells.

However, a further increase of the concentration of BCN to 2wt% in the composite leads to a dramatic decrease of the solar cell performance and all the performance related parameters including short-circuit current density (J_{sc}), V_{oc} and *FF* decrease significantly. A similar behaviour of carbon nanotube content dependent PV device was also observed in hybrid solar cells based on P3HT/SWNTs by Ren *et al*.[33] They found that there was an optimal concentration of carbon nanotubes in P3HT for efficient charge separation and transportation. Beyond this value, the device performance dropped significantly with an increase in carbon nanotube concentration.

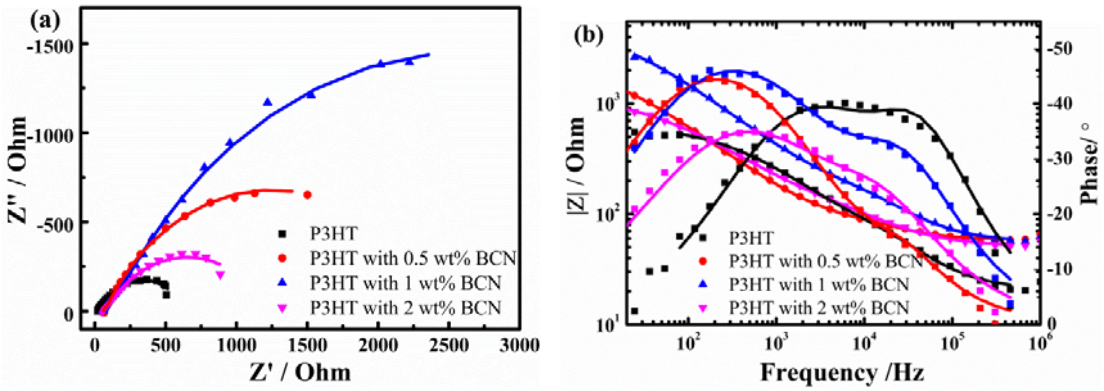

Figure 6. (a) Nyquist plots and (b) Bode plots of the perovskite solar cells with hole transport material containing different concentration of BCN in the P3HT measured at -0.8 V under dark condition.

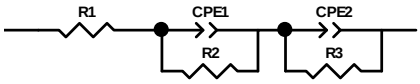

Scheme 1. Equivalent circuit used to fit the EIS spectrum of the perovskite solar cells.

R1: series resistance; R2/CPE1: charge transfer resistance and capacitance at HTM/Au ($R_{HTM/Au}$); R3/CPE2: Recombination resistance and associated capacitance of a perovskite solar cell (R_{ct}/C_{μ}).

In order to find out the reason for the different performance of the device with different content of BCN in the HTM composite, electrochemical impedance spectra (EIS) of the PSCs were measured and the Nyquist plots and Bode plots of the EIS are shown in Figure 6(a, b). An equivalent circuit (Scheme 1) which mimics the process of charge transport and recombination in perovskite solar cells was used to fit the impedance spectrum to extract the information on resistance for charge recombination, R_{ct} and chemical capacitance, C_{μ}.[26] The fitted data are shown in Table 3.

As shown in Figure 6(a) and Table 3, an increased R_{ct} of the PSCs with the addition of BCN in the HTM until 1wt% is observed. The R_{ct} of the device based on P3HT/(1wt% BCN) is nearly ten-fold higher than the recombination resistance of the cell based on pristine P3HT. Beyond this value, a further increase of BCN to 2wt% leads to the decrease of the recombination resistance. The effective electron lifetime, τ_n, which is the product of R_{ct} and C_{μ} ($\tau_n=R_{ct} \times C_{\mu}$) reflects the charge recombination rate in the solar cells. The longest τ_n is obtained with P3HT/(1wt% BCN) whereas the shortest electron lifetime is obtained with the pristine P3HT. It is found that the trend in the evolution of electron lifetime of the device with different BCN content is in good agreement with the change of the energy conversion efficiency and the V_{oc} of the cells, suggesting the change of the electron recombination may be responsible for the different device performance.

Since the general working principles of perovskite solar cells is similar to the well-known dye-sensitized solar cells using a solid state hole transport material,[36] the interfacial electron transfer from the TiO_2 nanoparticles or the perovskite material to the HTM is believed to be mainly responsible for the recombination in the device. In our case, however, besides the above recombination process, the BCN carbon nanotubes can provide additional pathway for electron recombination. It is known that carbon nanotubes are excellent electron acceptor. At a high content of BCN in the HTM composite (e.g. 2wt%), it is very likely that some carbon nanotubes may directly contact with the TiO_2 nanoparticle and with the perovskite material, causing electron transfer from TiO_2 and from the perovskite material to BCN. However, the electron that is transferred to BCN is confined in the HTM layer and is annihilated through recombination with hole of P3HT. This may explain the lower electron lifetime and lower performance of the device based on P3HT/(2wt% BCN) compared to the PSC with P3HT/(1wt% BCN). In addition, the negative effect of a higher content of carbon nanotubes (2wt%) in P3HT on the surface property of the HTM film is also clearly seen with the reduced grain sizes and increased density of cracks in the film compared to the HTM film

containing 1wt% BCN (Figure 4 (c, d)). The increased grain boundaries in P3HT/(2wt% BCN) composite could be another contributing factor for the increased charge recombination, leading to reduced device efficiency.

Table 3. Fitting parameters of the EIS results with PSC devices with different BCN content.

HTM	$R_{HTM/Au}(\Omega)$	R_{ct} (Ω)	C_{μ} (F)	τ_n (s)
P3HT	23.23	592	8.63E-06	0.0051
P3HT with 0.5 wt% BCN	58.02	2352	2.07E-05	0.0487
P3HT with 1 wt% BCN	57.6	5741	8.63E-06	0.0495
P3HT with 2 wt% BCN	51.02	1142	2.52E-05	0.0288

Since an efficient interfacial charge transport between $MAPbI_3$ perovskite and the HTM layer is crucial for the performance of perovskite solar cells, photoluminescence (PL) spectroscopy was employed to study the evolution of the interfacial charge transfer process of between the HTM film based on the prepared P3HT/BCN composites and $CH_3NH_3PbI_3$ perovskite light absorbing layer. The quenching behaviour in a PL spectrum is an indication of the dissociation of an exciton into an electron and a hole, which has been used to characterize the interfacial charge transfer in perovskite solar cell.[7,37,38] As shown in Figure 7(a), pure $MAPbI_3$ perovskite material shows a strong PL spectrum with a peak at around 735 nm due to the formation of high density of photo-generated exciton. This PL spectral peak decreases to around 5% of the pure $MAPbI_3$ when the perovskite film is interfaced with P3HT due to separation of the electron-hole pair (exciton) and transfer of hole from the perovskite material to P3HT. A further PL quenching is obtained when perovskite is interfaced with the HTM layers containing BCN (inset of Figure 7 (a)), suggesting an improved exciton dissociation and more efficient transport of charge across the $MAPbI_3$ perovsktie - HTM interface. In addition, compared to the PL of perovskite/ P3HT, the PL of the BCN containing composite is blue-shifted around 15 nm, which could be due to the interaction of BCN with P3HT in the HTM composite which might change the charge transport route. The BCN facilitated interfacial charge transfer is further confirmed by the time-resolved PL decay spectrum (Figure 7(b)). The PL decay is shortened from 10 ns to 5 ns when the MAPbI3 is interfaced with the P3HT/BCNs composite instead of the pristine P3HT, suggesting a faster interfacial charge transfer process. However, there is no significant difference in the PL spectrum of the $MAPbI_3$ interfaced with the HTM composites containing different content of BCNs (0.5 wt% - 2 wt%) in P3HT, indicating the limitation of carbon nanotubes in terms of improving the charge separation between the HTM and the perovskite light absorbing layer. This is further confirmed by the very similar PL intensity and decay time for the perovskite material which was interfaced with BCN only compared to the PL spectrum of the perovskite material. Therefore, the charge separation process at the perovskite/HTM composite should mainly occur between P3HT and MAPbI3 rather than BCN in the PSC device.

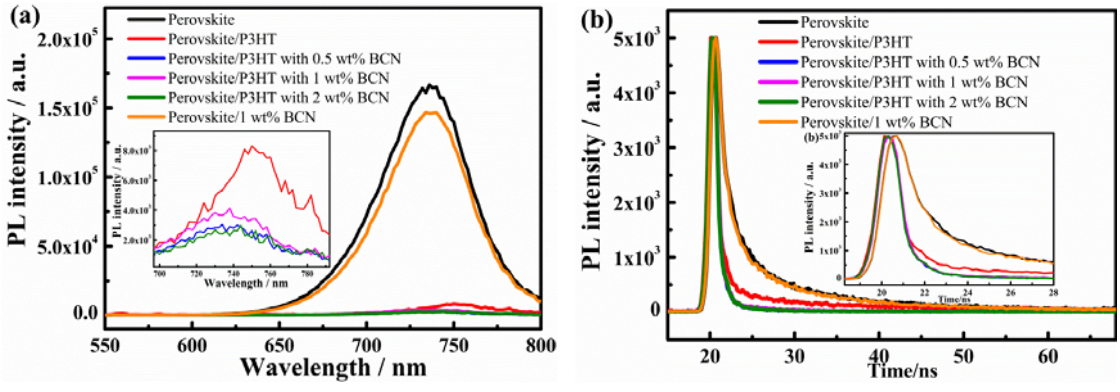

Figure 6. Photoluminescence (PL) spectrum as a function of wavelength (a) and time resolved PL decays (b) of perovskite/(P3HT/BCN composites) containing different content of bamboo-structure carbon nanotubes (BCN) and perovskite/(1 wt% BCN only).

Based on the result of the conductivity and interfacial charge transfer discussed above, clearly the significantly reduced performance of the perovskite solar cells containing a higher content of

bamboo-structure carbon nanotubes (2wt% BCN in P3HT) cannot be ascribed to the change of either the interfacial charge transfer between the perovskite layer and HTM layer or the charge mobility of the HTM since the P3HT/(2wt% BCNs) composite actually has similar PL quenching behaviour and hole conductivity compared to P3HT/(1wt% BCN). Instead, the higher charge recombination in the device should be responsible for the change of V_{oc} and the efficiency of the device as confirmed by the EIS study discussed above.

Conclusions

We have demonstrated the effect of the bamboo-structured carbon-nanotubes on the crystallinity, morphology and conductivity of the hole transport material based on P3HT and on the performance of corresponding perovskite solar cells (PSCs). Compared to the performance of PSC with pristine P3HT (maximum conversion efficiency η = 3.6% and average efficiency= (3.1±0.8)%), an over 200% increase of the light-to-electricity conversion efficiency was achieved with P3HT/(1wt% BCN) composite with η = 8.3% (average η = (7.6±1.16)%), mainly owing to the significant improved open circuit voltage and fill factor. The investigation on the morphology of the P3HT/BCN composite has confirmed that a continuous electron transport nano-network was formed in the composite where the BCNs were fully coated with a layer of P3HT polymer. Such nano-network structure was confirmed to be efficient for both electron transfer and transport. Over one order of magnitude enhancement of the electrical conductivity was obtained with the HTM composite containing BCNs beyond 1 wt% compared to the conductivity of the pristine P3HT based film. Time-dependent PL spectroscopy has indicated that the PL quenching was two times faster with the P3HT/BCN film interfaced with $MAPbI_3$ light absorbing layer, suggesting a more efficient charge separation at the interface of perovskite/HTM, thus reducing the interfacial charge carrier recombination in the device. The study of the composites by XRD, selected area electron diffraction and UV-visible spectroscopy and SEM all confirmed the improved crystallinity and gains of P3HT induced by bamboo-like carbon nanotubes (BCNs) induced. However, the performance of the PSCs strongly depends on the content of BCNs. A higher content of BCNs beyond 1wt% led to a significant decrease of the performance. The impedance spectroscopy has confirmed that the reduced electron recombination with the addition of BCN in the HTM layer was responsible for the change of the device performance. This research provided a new insight into the impact of HTM on the performance of perovskite solar cells and could lead to the development of new HTM for high efficiency PSCs.

Acknowledgements

The authors thank Australian Research Council (ARC) Future Fellowship scheme (FT 120100674) for the financial support for this work. Technical assistance from Mr Meng Zhang, University of Queensland for the PL measurements is acknowledged.

Notes and references

Address: School of Chemistry, Physics and Mechanical Engineering, Queensland University of Technology, Brisbane, QLD 4001, Australia.

(1) Lee, M. M.; Teuscher, J.; Miyasaka, T.; Murakami, T. N.; Snaith, H. J.: Efficient Hybrid Solar Cells Based on Meso-Superstructured Organometal Halide Perovskites. *Science* **2012**, *338*, 643-647.

(2) Kim, H. S.; Lee, C. R.; Im, J. H.; Lee, K. B.; Moehl, T.; Marchioro, A.; Moon, S. J.; Humphry-Baker, R.; Yum, J. H.; Moser, J. E.; Gratzel, M.; Park, N. G.: Lead Iodide Perovskite Sensitized All-Solid-State Submicron Thin Film Mesoscopic Solar Cell with Efficiency Exceeding 9%. *Scientific Reports* **2012**, *2*, 1-7.

(3) Burschka, J.; Pellet, N.; Moon, S. J.; Humphry-Baker, R.; Gao, P.; Nazeeruddin, M. K.; Gratzel, M.: Sequential deposition as a route to high-performance perovskite-sensitized solar cells. *Nature* **2013**, *499*, 316-319.

(4) Snaith, H. J.: Perovskites: The Emergence of a New Era for Low-Cost, High-Efficiency Solar Cells. *Journal of Physical Chemistry Letters* **2013**, *4*, 3623-3630.

(5) Gratzel, M.; Park, N. G.: ORGANOMETAL HALIDE PEROVSKITE PHOTOVOLTAICS: A DIAMOND IN THE ROUGH. *Nano* **2014**, *9*, 1440002.

(6) Huanping Zhou, Q. C., Hang Li, Song Luo, Tze-bing Song, Hsin-Sheng Duan, Ziruo Hong, Jingbi You, YongSheng Liu, Yang yang: Interface engineering of highly efficient perovskite solar cells. *Science* **2014**, *345*, 542-546.

(7) Stranks, S. D.; Eperon, G. E.; Grancini, G.; Menelaou, C.; Alcocer, M. J. P.; Leijtens, T.; Herz, L. M.; Petrozza, A.; Snaith, H. J.: Electron-Hole Diffusion Lengths Exceeding 1 Micrometer in an Organometal Trihalide Perovskite Absorber. *Science* **2013**, *342*, 341-344.

(8) Roiati, V.; Mosconi, E.; Listorti, A.; Colella, S.; Gigli, G.; De Angelis, F.: Stark Effect in Perovskite/TiO2 Solar Cells: Evidence of Local Interfacial Order. *Nano Letters* **2014**, *14*, 2168-2174.

(9) Marchioro, A.; Teuscher, J.; Friedrich, D.; Kunst, M.; van de Krol, R.; Moehl, T.; Gratzel, M.; Moser, J. E.: Unravelling the mechanism of photoinduced charge transfer processes in lead iodide perovskite solar cells. *Nature Photonics* **2014**, *8*, 250-255.

(10) Anyi Mei, X. L., Linfeng Liu, Zhiliang Ku, Tongfa Liu, Yaoguang Rong, Mi Xu, Min Hu, Jiangzhao Chen, Ying Yang, Michael Gratzel, Hongwei Han: A hole-conductor-free, fully printable mesoscopic perovskite solar cell with high stability. *Science* **2014**, *345*, 295-298.

(11) Colella, S.; Mosconi, E.; Fedeli, P.; Listorti, A.; Gazza, F.; Orlandi, F.; Ferro, P.; Besagni, T.; Rizzo, A.; Calestani, G.; Gigli, G.; De Angelis, F.; Mosca, R.: MAPbI(3-x) Cl-x Mixed Halide Perovskite for Hybrid Solar Cells: The Role of Chloride as Dopant on the Transport and Structural Properties. *Chemistry of Materials* **2013**, *25*, 4613-4618.

(12) Kojima, A.; Teshima, K.; Shirai, Y.; Miyasaka, T.: Organometal Halide Perovskites as Visible-Light Sensitizers for Photovoltaic Cells. *Journal of the American Chemical Society* **2009**, *131*, 6050-6051.

(13) Jeon, N. J.; Lee, J.; Noh, J. H.; Nazeeruddin, M. K.; Gratzel, M.; Seok, S. I.: Efficient Inorganic Organic Hybrid Perovskite Solar Cells Based on Pyrene Arylamine Derivatives as Hole-Transporting Materials. *Journal of the American Chemical Society* **2013**, *135*, 19087-19090.

(14) Qin, P.; Paek, S.; Dar, M. I.; Pellet, N.; Ko, J.; Gratzel, M.; Nazeeruddin, M. K.: Perovskite Solar Cells with 12.8% Efficiency by Using Conjugated Quinolizino Acridine Based Hole Transporting Material. *Journal of the American Chemical Society* **2014**, *136*, 8516-8519.

(15) Qin, P.; Tanaka, S.; Ito, S.; Tetreault, N.; Manabe, K.; Nishino, H.; Nazeeruddin, M. K.; Gratzel, M.: Inorganic hole conductor-based lead halide perovskite solar cells with 12.4% conversion efficiency. *Nature Communications* **2014**, *5*, 3834.

(16) Bi, D. Q.; Yang, L.; Boschloo, G.; Hagfeldt, A.; Johansson, E. M. J.: Effect of Different Hole Transport Materials on Recombination in CH3NH3PbI3 Perovskite-Sensitized Mesoscopic Solar Cells. *Journal of Physical Chemistry Letters* **2013**, *4*, 1532-1536.

(17) Obrzut, J.; Page, K. A.: Electrical conductivity and relaxation in poly(3-hexylthiophene). *Physical Review B* **2009**, *80*, 195211.

(18) Sirringhaus, H.; Brown, P. J.; Friend, R. H.; Nielsen, M. M.; Bechgaard, K.; Langeveld-Voss, B. M. W.; Spiering, A. J. H.; Janssen, R. A. J.; Meijer, E. W.; Herwig, P.; de Leeuw, D. M.: Two-dimensional charge transport in self-organized, high-mobility conjugated polymers. *Nature* **1999**, *401*, 685-688.

(19) Li, L. G.; Lu, G. H.; Yang, X. N.: Improving performance of polymer photovoltaic devices using an annealing-free approach via construction of ordered aggregates in solution. *Journal of Materials Chemistry* **2008**, *18*, 1984-1990.

(20) Geng, J. X.; Zeng, T. Y.: Influence of single-walled carbon nanotubes induced crystallinity enhancement and morphology change on polymer photovoltaic devices. *Journal of the American Chemical Society* **2006**, *128*, 16827-16833.

(21) Schuettfort, T.; Snaith, H. J.; Nish, A.; Nicholas, R. J.: Synthesis and spectroscopic characterization of solution processable highly ordered polythiophene-carbon nanotube nanohybrid structures. *Nanotechnology* **2010**, *21*, 025201.

(22) Le, A. P.; Huang, T. M.; Chen, P. T.; Yang, A. C. M.: Synthesis and Optoelectronic Behavior of Conjugated Polymer Poly(3-hexylthiophene) Grafted on Multiwalled Carbon Nanotubes. *Journal of Polymer Science Part B-Polymer Physics* **2011**, *49*, 581-590.

(23) Song, T.; Lee, S. T.; Sun, B. Q.: Prospects and challenges of organic/group IV nanomaterial solar cells. *Journal of Materials Chemistry* **2012**, *22*, 4216-4232.

(24) Wang, H. X.; Peter, L. M.: Influence of Electrolyte Cations on Electron Transport and Electron Transfer in Dye-Sensitized Solar Cells. *Journal of Physical Chemistry C* **2012**, *116*, 10468-10475.

(25) Liu, M. N.; Wang, H. X.; Yan, C.; Will, G.; Bell, J.: One-step synthesis of titanium oxide with trilayer structure for dye-sensitized solar cells. *Applied Physics Letters* **2011**, *98*, 133113.

(26) Dualeh, A.; Moehl, T.; Tetreault, N.; Teuscher, J.; Gao, P.; Nazeeruddin, M. K.; Gratzel, M.: Impedance Spectroscopic Analysis of Lead Iodide Perovskite-Sensitized Solid-State Solar Cells. *Acs Nano* **2014**, *8*, 362-373.

(27) Saini, V.; Li, Z. R.; Bourdo, S.; Dervishi, E.; Xu, Y.; Ma, X. D.; Kunets, V. P.; Salamo, G. J.; Viswanathan, T.; Biris, A. R.; Saini, D.; Biris, A. S.: Electrical, Optical, and Morphological Properties of P3HT-MWNT Nanocomposites Prepared by in Situ Polymerization. *Journal of Physical Chemistry C* **2009**, *113*, 8023-8029.

(28) Saito, R.; Hofmann, M.; Dresselhaus, G.; Jorio, A.; Dresselhaus, M. S.: Raman spectroscopy of graphene and carbon nanotubes. *Advances in Physics* **2011**, *60*, 413-550.

(29) Ren, S.; Bernardi, M.; Lunt, R. R.; Bulovic, V.; Grossman, J. C.; Gradečak, S.: Toward Efficient Carbon Nanotube/P3HT Solar Cells: Active Layer Morphology, Electrical, and Optical Properties. *Nano Letters* **2011**, *11*, 5316-5321.

(30) Musumeci, A. W.; Silva, G. G.; Liu, J. W.; Rintoul, L.; Waclawik, E. R.; George, G. A.: MWNT polymer nanocomposites based on P3HT. In *Advanced Materials and Processing Iv*; Zhang, D., Pickering, K., Gabbitas, B., Cao, P., Langdon, A., Torrens, R., Verbeek, J., Eds.; Trans Tech Publications Ltd: Stafa-Zurich, 2007; Vol. 29-30; pp 291-294.

(31) Musumeci, A. W.; Silva, G. G.; Liu, J.-W.; Martens, W. N.; Waclawik, E. R.: Structure and conductivity of multi-walled carbon nanotube/poly(3-hexylthiophene) composite films. *Polymer* **2007**, *48*, 1667-1678.

(32) Giulianini, M.; Waclawik, E. R.; Bell, J. M.; De Crescenzi, M.; Castrucci, P.; Scarselli, M.; Motta, N.: Regioregular poly(3-hexyl-thiophene) helical self-organization on carbon nanotubes. *Applied Physics Letters* **2009**, *95*.

(33) Ren, S. Q.; Bernardi, M.; Lunt, R. R.; Bulovic, V.; Grossman, J. C.; Gradecak, S.: Toward Efficient Carbon Nanotube/P3HT Solar Cells: Active Layer Morphology, Electrical, and Optical Properties. *Nano Letters* **2011**, *11*, 5316-5321.

(34) Osaka, M.; Benten, H.; Lee, L. T.; Ohkita, H.; Ito, S.: Development of highly conductive nanodomains in poly(3-hexylthiophene) films studied by conductive atomic force microscopy. *Polymer* **2013**, *54*, 3443-3447.

(35) Di Giacomo, F.; Razza, S.; Matteocci, F.; D'Epifanio, A.; Licoccia, S.; Brown, T. M.; Di Carlo, A.: High efficiency CH3NH3PbI((3-x))Cl-x, perovskite solar cells with poly(3-hexylthiophene) hole transport layer. *Journal of Power Sources* **2014**, *251*, 152-156.

(36) Gonzalez-Pedro, V.; Juarez-Perez, E. J.; Arsyad, W. S.; Barea, E. M.; Fabregat-Santiago, F.; Mora-Sero, I.; Bisquert, J.: General Working Principles of CH3NH3PbX3 Perovskite Solar Cells. *Nano Letters* **2014**, *14*, 888-893.

(37) Zhang, M.; Yu, H.; Lyu, M.; Wang, Q.; Yun, J.-H.; Wang, L.: Composition-dependent photoluminescence intensity and prolonged recombination lifetime of perovskite CH3NH3PbBr3-xClx films. *Chemical Communications* **2014**.

(38) Zhong, Q.; Diev, V. V.; Roberts, S. T.; Antunez, P. D.; Brutchey, R. L.; Bradforth, S. E.; Thompson, M. E.: Fused Porphyrin-Single-Walled Carbon Nanotube Hybrids: Efficient Formation and Photophysical Characterization. *Acs Nano* **2013**, *7*, 3466-3475.